

Printing of Responsive Photonic Cellulose Nanocrystal Microfilm Arrays


Tianheng H. Zhao, Richard M. Parker, Cyan A. Williams, Kevin T. P. Lim, Bruno Frka-Petescic, and Silvia Vignolini*

Interactive materials capable of changing appearance upon exposure to external stimuli, such as photonic inks, are generally difficult to achieve on a large scale as they often require self-assembly processes that are difficult to control macroscopically. Here this problem is overcome by preparing arrays of cellulose nanocrystal (CNC) microfilms from discrete nanoliter sessile droplets. The obtained microfilms show extremely uniform and intense color, enabling exceptional consistency in optical appearance across the entire array. The color can be controlled through the initial ink formulation, enabling the printing of polychromatic dot-matrix images. Moreover, the high surface-to-volume ratio of the microfilms and the intrinsic hydrophilicity of the natural building block allow for a dramatic real-time colorimetric response to changes in relative humidity. The printed CNC microfilm arrays overcome the existing issues of scalability, optical uniformity, and material efficiency, which have held back the adoption of CNC-based photonic materials in cosmetics, interactive-pigments, or anticounterfeit applications.

1. Introduction

Cellulose is one of the most abundant natural substances and has played a crucial role in human history, with uses ranging from cotton clothing to paper manufacture. Recently, its nanoscale derivatives, namely cellulose nanocrystals (CNCs) and nanofibers (CNFs), have gained popularity for their unique capability to combine biocompatibility and sustainability with exceptional optical properties. Starting with these natural building blocks and using only self-assembly techniques, it is possible to achieve a wide variety of different functionalities

T. H. Zhao, Dr. R. M. Parker, C. A. Williams, K. T. P. Lim,
Dr. B. Frka-Petescic, Dr. S. Vignolini
Department of Chemistry
University of Cambridge
Lensfield Road, CB2 1EW Cambridge, UK
E-mail: sv319@cam.ac.uk

 The ORCID identification number(s) for the author(s) of this article can be found under <https://doi.org/10.1002/adfm.201804531>.

© 2018 The Authors. Published by WILEY-VCH Verlag GmbH & Co. KGaA, Weinheim. This is an open access article under the terms of the Creative Commons Attribution License, which permits use, distribution and reproduction in any medium, provided the original work is properly cited. The copyright line of this paper was changed on 26 February 2019 after initial publication.

DOI: 10.1002/adfm.201804531

ranging from transparent^[1] or highly scattering materials,^[2] to photonic pigments.^[3,4]

When dispersed in water, colloidal CNCs can spontaneously organize into a cholesteric liquid crystalline phase above a critical concentration.^[5–7] Upon drying, this ordering is preserved, giving rise to a helicoidal nanoarchitecture in the solid-state. Importantly, the periodicity of this helicoid can be adjusted to the order of the wavelength of visible light, resulting in vivid, iridescent structural color.^[7,8] The reflected color is dependent on the pitch, p , the average refractive index, \bar{n} , and the orientation of the helical axis, \mathbf{m} , while the visual appearance (e.g., matt/metallic) is dictated by the domain structure. The precise control of both the pitch and orientation of the CNC domains is crucial for scalable manufacturing of

CNC-based photonic materials, but it remains challenging to stringently control the organization and alignment of the cholesteric phase.^[9–11] To overcome this challenge, various approaches have been proposed to improve the long-range homogeneity of the self-assembled structure, such as using external fields^[8] or geometrical confinement.^[12,13]

2. Results and Discussion

Inspired by the offset printing technique,^[14] here we report a method to produce homogeneous centimeter-scale arrays of monochromatic CNC microfilms. As shown in **Figure 1a**, rectangular arrays of blue, green, and red circular CNC microfilms with individual diameters, \varnothing , of 600 and 1000 μm were printed onto a hydrophilic/hydrophobic-patterned glass slide.^[15,16] The size, location, and shape of the individual films were defined by the initial array of nanoliter sessile droplets, itself formed by the selective dewetting of a larger drop of aqueous CNC suspension. Each array uniformly reflects a single color, which is predetermined solely by the salt concentration of the CNC suspension.^[5,17] Vivid structural color appeared only at the specular reflection (**Figure S1**, Supporting Information), indicating well-aligned domains within the microfilms.^[8,9,11] The arrays are highly iridescent, with the color strongly blue-shifting with increasing viewing angle (**Figure 1b**). **Figure 1c** shows a more complex dot matrix image of a “Christmas tree,” viewed through

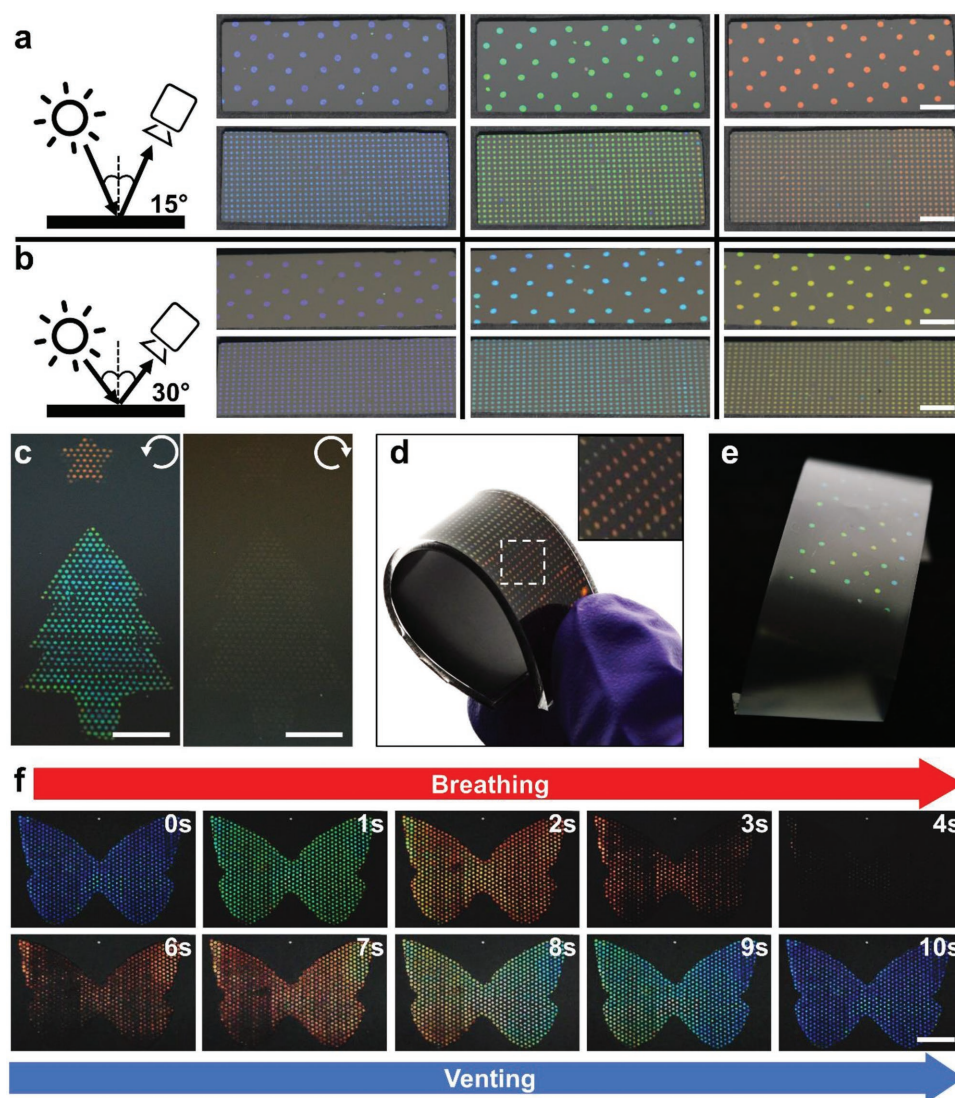


Figure 1. a,b) Photographs of uniform red, green, and blue arrays of CNC microfilms deposited onto a patterned glass substrate, with individual microfilm diameters of 1000 μm (top) and 600 μm (bottom). As the viewing angle is increased from (a) 15° (relative to the normal) to (b) 30° the arrays are observed to iridescently blue-shift, characteristic of a well-ordered 1D photonic structure. c) A “Christmas tree” dot matrix image consisting of both red and green arrays of 600 μm CNC microfilms is clearly visible when imaged through a left-handed circular polarizer, but not visible through a right-handed circular polarizer. d) A CNC microfilm array prepared on a flexible PDMS substrate. e) An array of CNC microfilms was transferred onto adhesive tape. f) A blue “butterfly” dot matrix image rapidly and reversibly changed color in response to the moisture in an exhaled breath. All scale bars correspond to 5 mm.

circular polarizers. By using two different “CNC inks,” areas with different colors were deposited simultaneously within the same array. Due to the inherent left-handedness of the helical CNC architecture, the microfilms reflect only left-handed circularly polarized (LCP) light and therefore the image could be revealed or hidden using simple circular polarization filters. The absence of any reflectance in the right-handed circular polarization (RCP) is further evidence of highly-ordered and well-aligned films.^[7,18] This versatile method can be used to deposit CNC microfilm arrays onto a range of silanizable substrates, exemplified with silicon in Figure S2 (Supporting Information) and flexible polydimethylsiloxane (PDMS) in Figure 1d. In the latter case, the CNC films can withstand the deformation of the PDMS without cracking or detaching, contrasting strongly with

dish-cast CNC films that are often brittle and prone to breaking during handling.^[19,20] Such resistance to cracks is mainly due to their thinness (<5 μm) and to the discontinuous nature of the patterned array. Additionally, adhesive tape can be used to detach the array (Figure 1e), enabling transfer to a wider range of substrates. The CNC microfilms are interactive, exhibiting a dramatic, real-time colorimetric response to changes in humidity. As shown in Figure 1f, a “butterfly” dot matrix image changed from blue, through green and red, to infra-red upon exhaling onto the sample ($t = 0\text{--}4$ s). Once the exposure to humid breath stopped, the CNC films quickly recovered their original blue color ($t = 6\text{--}10$ s).

The method to prepare arrays of CNC films is illustrated schematically in Figure 2 and can be divided into three key

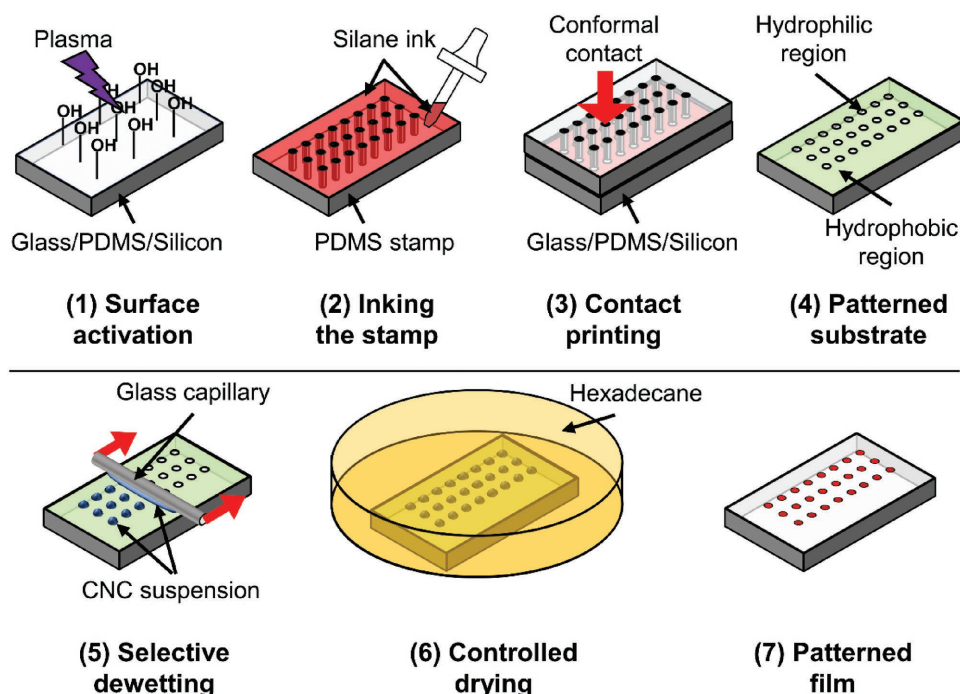


Figure 2. Schematic describing the preparation of a CNC microfilm array: (1–4) Microcontact printing of octadecyltrichlorosilane (OTS) patterns the hydrophilic substrate with hydrophobic regions. (5) A drop of CNC suspension is dispersed into an array of sessile nanodroplets by blade coating and selective dewetting. (6–7) The droplets are slowly dried under hexadecane oil to produce a uniform array of CNC microfilms.

stages: i) preparing a hydrophilic/hydrophobic patterned surface by microcontact printing, ii) forming a sessile CNC droplet array by selective dewetting, and iii) slowly drying the droplets under an immiscible layer of hexadecane oil to form a CNC microfilm array. The third fabrication step is vital to obtain highly uniform microfilms via a self-assembly process. The optical appearance of a CNC droplet rapidly dried in the ambient environment ($t < 5$ min, Figure 3a) is very different to an equivalent droplet dried slowly under immiscible hexadecane ($t \leq 2$ d, Figure 3b). Due to their large surface-to-volume ratio, pinned sessile droplets dried in the ambient environment had a faster evaporation rate at the edge than the center, resulting in an outward capillary flow. This outward flow deposited the colloidal CNCs near the edge of the droplet resulting in a dry microfilm with the profile described in Figure 3c, which is commonly known as a “coffee stain.”^[21,22] The radial shear also disrupted the organization of the CNCs,^[23–25] with many tilted domains observed in dark-field microscopy (Figure S3a, Supporting Information). In contrast, droplets dried slowly under hexadecane experience uniform water loss across the droplet surface, resulting in a negligible capillary flow. As such, the slowly dried microfilms exhibit a dome-shaped cross-sectional profile (Figure 3d), with typical heights of 1.8 and 3.5 μm for microfilms dried from 600 and 1000 μm diameter droplets,

respectively (Figure S4, Supporting Information). Most importantly, these films present an extremely well-aligned internal architecture, with no disruption at the edge, leading to the optimum photonic response across the film (Figure 3b).

Scanning electron microscope (SEM) images of the cross-section of a typical microfilm confirmed that the highly-ordered, monodomain structure extends from the center to the edge (Figure 4).

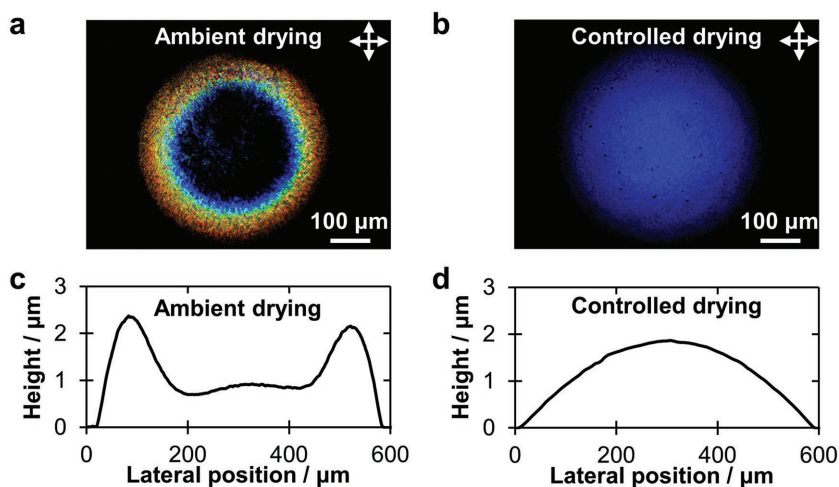


Figure 3. a,b) Cross-polarized reflection images of CNC microfilms ($\varnothing = 600$ μm) showing (a) the inhomogeneous, speckled color arising from the “coffee ring” deposition and radial shearing that occurred under ambient drying conditions and (b) the uniform color produced upon slowly drying in a controlled environment. c,d) Corresponding cross-sectional profiles of the microfilms in panels (a,b), as measured by stylus profilometry.

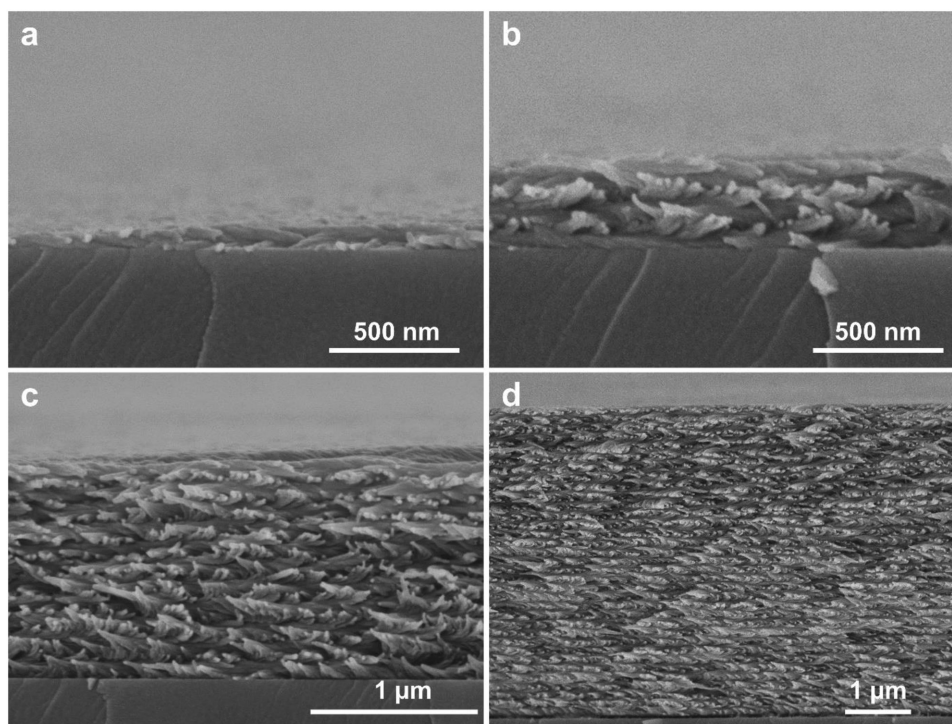


Figure 4. a–d) SEM images of the cross-section of a typical microfilm from (a) the edge to (d) the centre, showing a highly-ordered, monodomain structure with little defects.

To understand the formation of uniform color in CNC microfilms, a time-lapse of a droplet drying under hexadecane was recorded (Figure S5, Supporting Information). Initially, multiple birefringent cholesteric domains were randomly orientated throughout the sessile droplet. Strong planar anchoring of the local director \mathbf{n} on both liquid–substrate and liquid–liquid interfaces favors the alignment of the helical axis \mathbf{m} locally perpendicular to both. The high aspect ratio of the deposited droplet made the top interface nearly parallel to the horizontal substrate, resulting in a uniform vertical alignment of \mathbf{m} throughout the sessile droplet,^[12,13,27] as confirmed by the disappearance of the birefringent features within 80 min. The slow drying rate allowed neighboring domains to merge to form a single large cholesteric domain, with possible trapped defects and disclinations.^[7,26] During the last hour of drying, the film became dark red before gradually shifting to its final blue color. Although a single nanoliter droplet took up to two days to dry by this method, the drying time required to produce large arrays of high-quality microfilms remains the same. Furthermore, the crucial droplet surface-to-volume ratio that allows anchoring to dominate is unaffected by the scale of the array.

During the drying process, we observed that some droplets depinned from the hydrophilic/hydrophobic boundary. Once depinned, further loss of water led the droplet to contract both vertically and laterally. As shown in **Figure 5**, the colors of such microfilms are significantly red-shifted upon depinning, with

the extent of the color-shift dependent on the lateral contraction of the film. Much like that reported for spherical microdroplets^[12]; upon reaching a kinetically-arrested state this additional lateral contraction leads to reduced vertical compression exerted along the helicoidal axis, \mathbf{m} , resulting in an apparent increase of the final pitch, p . To guarantee depinning did not occur upon drying, we systematically employed a sacrificial CNC coating step (see Experimental Section and Figure S6 (Supporting Information)), that allowed for the reliable and repeatable fabrication of large area CNC microfilm arrays with uniform color.

Cross-polarized optical images of representative CNC microfilms are shown in **Figure 6a–f**, with all other polarization configurations shown in Figure S3b,c (Supporting Information).

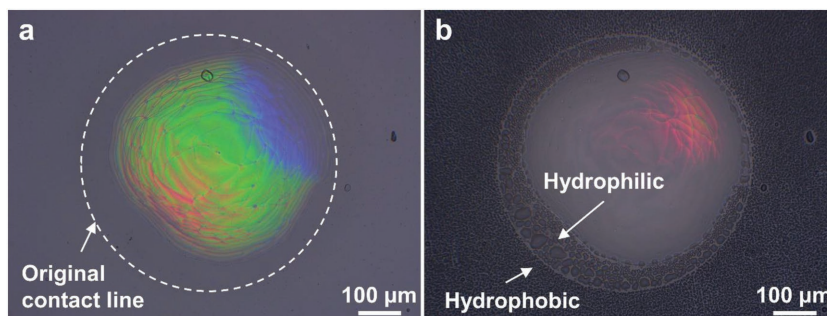


Figure 5. Images of a purportedly blue CNC microfilm ($\varnothing = 600 \mu\text{m}$) that has partially depinned from the hydrophobic–hydrophilic contact line. a) The microfilm shows regions of different color depending on the amount of lateral contraction from the initial contact line. b) Condensation on the surface clearly visualizes the boundary between hydrophobic and hydrophilic regions, allowing the degree of contraction to be determined. Note that in panel (b) the microfilm has color-shifted into the infrared due to ingress of moisture.

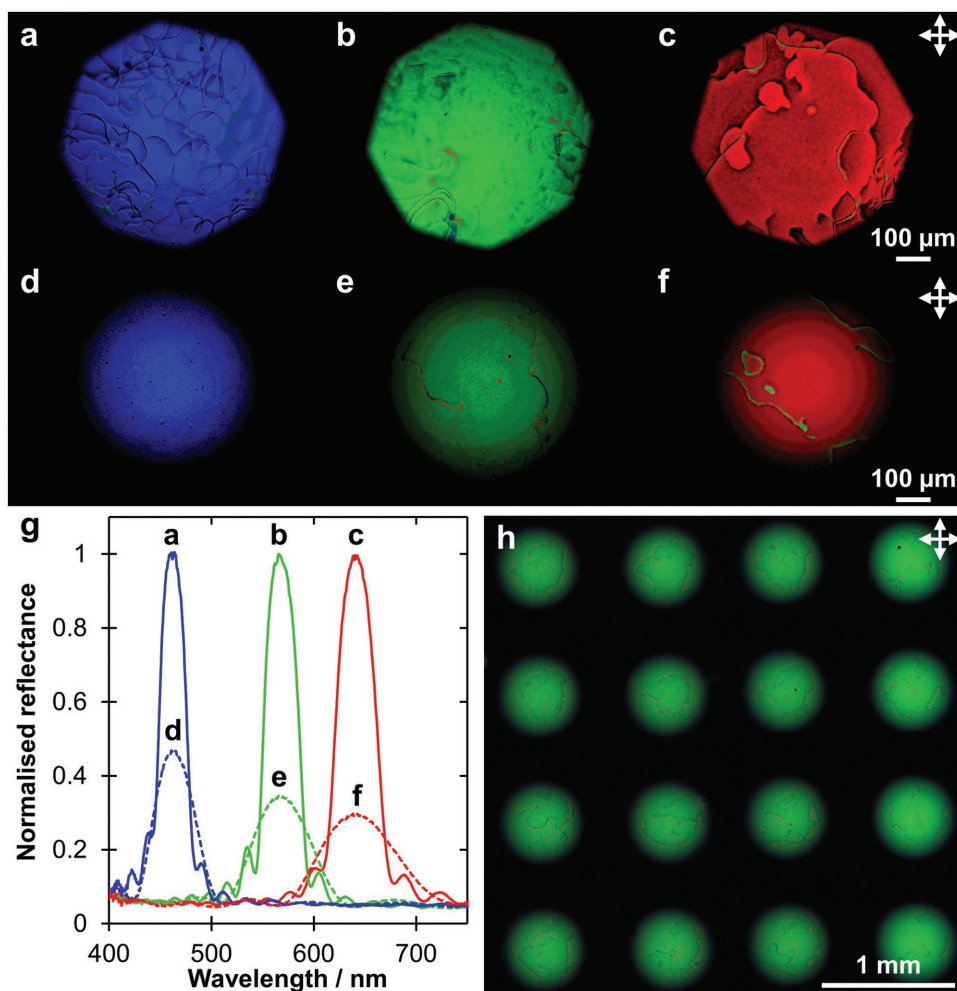


Figure 6. a–f) Cross-polarized reflection micrographs of blue, green and red CNC microfilms with a diameter of (a–c) 1000 μm and (d–f) 600 μm . g) Corresponding reflectance spectra for panels (a–f) collected through a left-handed circular polarizer, with the intensity normalized against a silver mirror. h) Stitched images showing a larger area of the uniformly green CNC microfilm array ($\varnothing = 600 \mu\text{m}$).

Cross-polarization allows for the selective imaging of the color reflected from the helicoidal nanostructure by subtracting the thin-film interference fringes. A color shift was observed adjacent to disclination lines, where the local ordering has been disturbed by trapped defects or dust. No tilted domains were observed under dark-field illumination (Figure S3b,c, Supporting Information). The corresponding reflection spectra are shown in Figure 6g; the spectra were recorded at the center of each microfilm, collected through a left-handed circular polarizer and referenced against a silver mirror (i.e., a perfect left-handed cholesteric sample would have 100% reflectance in its photonic band gap). For microfilms with a diameter of 1000 μm , the peak reflectance could reach this theoretical limit, while microfilms with a diameter of 600 μm have a reflectance of up to 50%. The peak intensity reduction from the blue to the red microfilm is attributed to the weakened interference arising from the decreased number of pitch repeats for a fixed thickness. For comparison, reflection spectra recorded in RCP showed no peak (Figure S7b, Supporting Information). The film-to-film uniformity across the CNC microfilm array is illustrated in the stitched images in Figure 6h and Figure S8

(Supporting Information). The microfilms demonstrate much better material efficiency in comparison to thicker dish-cast films due to the high reflectivity arising from the well-ordered nanoarchitecture as well as the suppression of edge effects.^[7,11,20,28]

The high dynamic sensitivity of the CNC microfilms to humidity is due to the reduced thickness and the perfect alignment of **m** across the microfilms, as compared to dish-cast CNC films.^[20,29] This is exemplified in Movie S1 (Supporting Information), where the moisture released from a fingertip is shown to be sufficient to shift a blue array to infrared in seconds. To quantify this behavior, the peak wavelength shift for a blue CNC microfilm ($\varnothing = 1000 \mu\text{m}$) was tracked upon three cycles of 0% \leftrightarrow 75% relative humidity (RH) at 20 $^{\circ}\text{C}$. As shown in Figure 7a, a 50 nm red-shift with negligible hysteresis was observed upon cycling the relative humidity over this range. The blue, green, and red CNC microfilms ($\varnothing = 1000 \mu\text{m}$) all red-shifted by $\approx 11\%$ with respect to the initial peak wavelength over this humidity range (Figure S9a, Supporting Information). The colorimetric response is not caused by a change in temperature, as confirmed by the stable peak wavelength upon heating

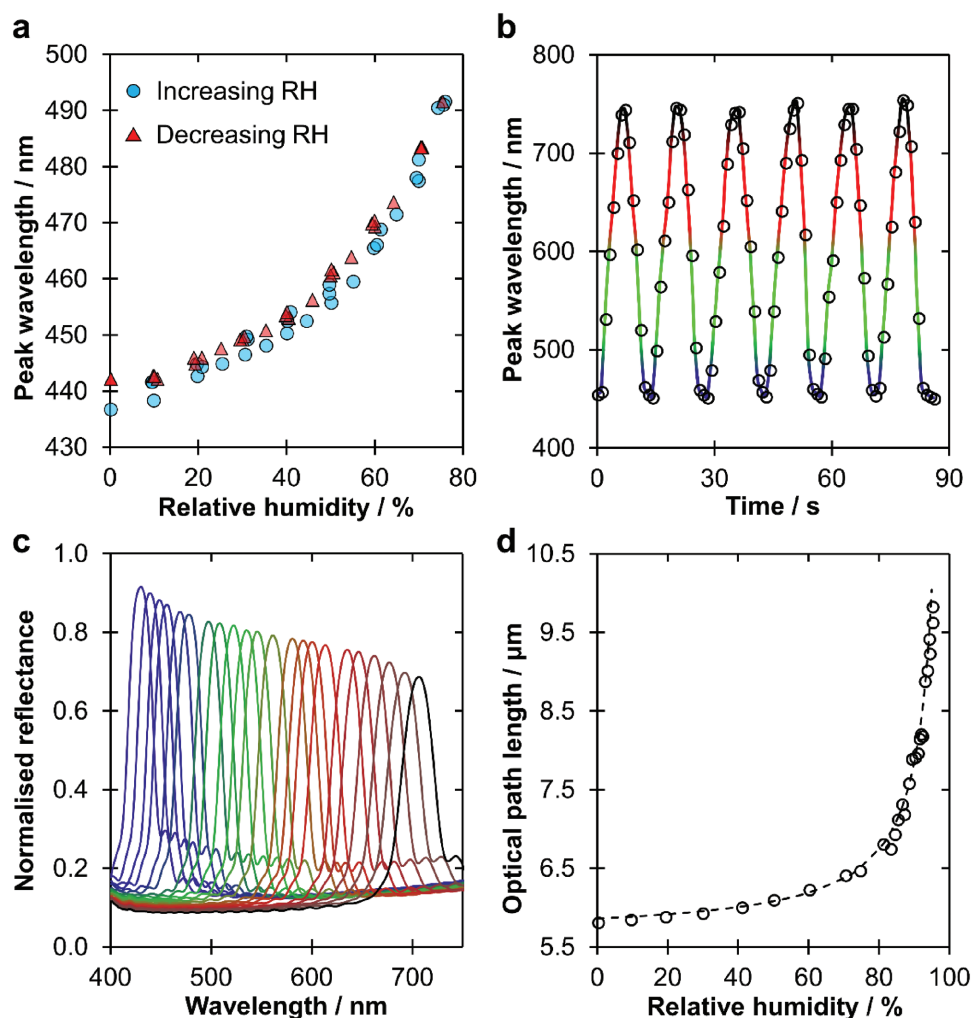


Figure 7. a) The peak wavelength shift of a blue CNC microfilm to changes in relative humidity (0% \leftrightarrow 75% RH), with little hysteresis observed over three cycles of (●) increasing and (▲) decreasing RH. b) The reproducible and large peak wavelength shift of a CNC microfilm subject to six cycles of rapid humidity change (0% \leftrightarrow 100% RH). c) The colorimetric response of a blue CNC microfilm ($\varnothing = 1000 \mu\text{m}$) upon changing the relative humidity stepwise from 0% to 95% RH. The spectra were taken through a left-handed circular polarizer, and the intensity was normalized against a silver mirror. d) The optical path length (l_{opt}), as calculated from the thin-film interference, increased by 70% upon increasing from 0% to 95% RH.

the sample from 20 to 60 °C at 0% RH (Figure S9b, Supporting Information). Furthermore, upon locally heating the sample from 20 to 60 °C under a constant humid nitrogen flow (75% RH at 20 °C, corresponding to $12.94 \text{ g(H}_2\text{O)} \text{ m}^{-3}$), the microfilm shifted to a lower wavelength, confirming that the film is sensitive to relative humidity rather than absolute humidity (Figure S9c, Supporting Information).

To explore the responsiveness of the CNC film array to large changes in relative humidity (0% \leftrightarrow 100% RH), the local environment was rapidly alternated six times between saturated and dry atmospheres over a period of 90 s (Figure 7b; Movie S2, Supporting Information), during which the peak wavelength reversibly and repeatedly shifted by $\approx 300 \text{ nm}$. This much greater peak shift corresponds to an increasing rate of water uptake for CNC films at higher RH, as previously demonstrated by the weight increase of dish-cast CNC films in a humid environment.^[20] Moreover, the thin CNC microfilms have complete water penetration and require only

minimal water uptake for instantaneous color shifts ($< 1 \text{ s}$), in contrast to other reported CNC-based films (typically minutes to hours).^[20,30]

Figure 7c shows the change in reflected color of a blue microfilm when subjected to 0%–95% RH. As CNC films are known to have negligible porosity,^[31] such color change can be attributed to the swelling of the film upon water uptake. The slight decrease of the reflectance with increasing humidity is attributed to the decrease of overall birefringence, as the birefringent CNCs were diluted with isotropic water. To quantify the swelling, the corresponding change of the optical path length, l_{opt} , was measured from thin-film interference spectral fringes (see the Experimental Section and Figure S10 in the Supporting Information). As shown in Figure 7d, increasing the humidity from 0% to 95% RH, resulted in l_{opt} increasing by a factor of 1.7. Upon water infiltration, the average refractive index, \bar{n} , of the CNC microfilms must decrease and as the thickness is given by $h = l_{opt} / \bar{n}$, it can be concluded that the

swollen film contains at least 41 vol% of water. This amount of water uptake, although large, is insufficient to rehydrate the CNCs beyond a kinetically-arrested gel. This explains why the microfilms can be repeatedly subjected to rapid swelling without disruption of the underlying nanostructure.

3. Conclusion

In conclusion, we have developed a scalable printing method to produce arrays of structurally colored CNC microfilms from spatially-defined nanoliter sessile droplets. Complex dot matrix images were designed by controlling the size and location of individual CNC microfilms via micropatterning of the substrate. By employing slow evaporation, the deposition and self-assembly of the CNCs were not disrupted by commonly observed shear or “coffee-ring” effects. When combined with strong anchoring of the CNCs to the substrate, this resulted in a highly-ordered, monodomain structure with little to no defects (e.g., Figure 6d–f). Our method enables the fabrication of responsive microfilms with high reflectivity, where the color is deterministically controlled by the CNC ink formulation. Finally, the instantaneous, reversible colorimetric response, from ultraviolet to infrared, opens new pathways for CNC-based responsive photonic pigments to be used in decorative, sensing, or anticounterfeiting applications.

4. Experimental Section

Characterization: Photographs were taken with a digital camera (D3200, Nikon), mounted with a left-handed circular polarizer (CIR-PL, Hoya). Polarized optical images were collected with a customized ZEISS Axio scope A1 microscope in reflection mode using a Halogen lamp (ZEISS HAL100) as a light source in Koehler illumination. The reflected light could also be filtered with a quarter wave plate and a linear polarizer mounted at different orientations to distinguish LCP or RCP light. A beam splitter directed the filtered light to a CCD camera (UI-3580LE-C-HQ, IDS) and an optical fiber (core diameter 50 μm) that was mounted in confocal configuration to collect microspectroscopic data (AvaSpec-HS2048 spectrometer, Avantes). All spectra were normalized to the reflection spectrum of a silver mirror (Thorlabs, PF10-03-P01) in LCP unless stated otherwise. All bright-field images were taken with a ZEISS EC Epiplan-Apochromat objective (10x NA 0.3) and dark-field images were taken with a ZEISS EC Epiplan-Apochromat objective (20x NA 0.6). The stitched images were taken by scanning over a 16 mm² area with a ZEISS EC Epiplan-Neofluar objective (5x NA 0.13). Scanning electron microscope (SEM) images were collected with a Mira3 system (TESCAN) operated at 3 kV and a working distance of 4–5 mm. The samples were mounted on aluminum stubs using conductive carbon tape and coated with a 10 nm thick layer of platinum with a sputter coater (Quorum Q150T ES).

CNC Suspension: The cellulose nanocrystal suspension was prepared as described previously.^[8] In short, Whatman No. 1 cellulose filter paper (30 g) was hydrolyzed with sulfuric acid (64 wt%, 420 mL, VWR) for 30 min at 66 °C and then quenched by dilution with cold Milli-Q water. After removing most of the acid and supernatant by centrifugation, the suspension was dialyzed against deionized water (MWCO 12–14 kDa). The suspension was tip sonicated in an ice bath (Fisherbrand Ultrasonic disintegrator 500 W, amplitude 30% max, 5000 J g⁻¹ of CNC). The final suspension was concentrated through a dialysis membrane (MWCO 12–14 kDa) using an osmotic bath of poly(ethylene glycol) (35 kDa, Sigma-Aldrich). The final measured concentration was 14.5 wt%. The stock suspension was diluted with

Milli-Q water and sodium chloride (0.1 M) to obtain suspensions with 8.1 wt% of CNC and [NaCl]/[CNC] ratio of 25, 50, and 100 mmol kg⁻¹. The suspensions were equilibrated for 7 d to allow phase separation, and the denser anisotropic phase was used.

Stamp Preparation by Soft Lithography and Punch: Stamps with 600 μm features were prepared by casting PDMS (SYLGARD 184, 10: 1 w/w precursor: crosslinker) onto a master fabricated via photolithography. Stamps with 1000 μm features were prepared by punching holes through a sheet of PDMS using a 1.0 mm biopsy punch (BPP-10F, kai medical).

Patterned Substrates by Microcontact Printing: Glass and silicon substrates were rinsed with ethanol and blown dry with nitrogen gas. Polydimethylsiloxane (PDMS) substrates were cleaned by tape (Scotch Magic tape, 3M). The substrates were then activated with a plasma cleaner (Femto, Diener electronic) for 8 s (glass) or 32 s (PDMS), rendering the whole surface hydrophilic. 25 μL of 5% v/v octadecyltrichlorosilane (OTS, Sigma-Aldrich) solution in hexadecane (Sigma-Aldrich) was spread across a 90 mm petri dish using a swab (Absorb-Tip Foam Swab, Techspray). Stamps were inked by conformal contact with the coated petri dish for 30 s. The inked stamp was then applied conformally to the activated substrate for 60 s. After treatment, the contacted surface was rendered hydrophobic while the untouched areas remained hydrophilic. The contact angle of a 0.5 μL water droplet was <5° for the freshly plasma-treated glass and 102° for the OTS-treated surface.

CNC Microfilm Arrays by Blade Coating and Selective Dewetting: A customized blade-coating set-up was prepared using a glass capillary placed on top of a glass slide, with a coverslip (thickness 0.13–0.16 mm) used as a spacer. The CNC suspension was prepared as previously reported and is described in the Supporting Information.^[8] A drop of CNC suspension (10 μL) was pipetted near one end of the patterned substrate. By sliding the “blade” across the substrate, the CNC suspension broke into many small sessile droplets, defined by the hydrophobic boundaries of the prepatterned substrate. To enforce pinning, sacrificial CNC films were first produced, whereby the wetted substrate was immediately placed on a hot plate (SD162, Stuart Equipment) at 55 °C. Once dry, the sacrificial CNC films were removed by rinsing with milli-Q water, followed by gentle wiping with damp tissue (White Medical Wipes, Kimberly Clark). Scanning electron microscope (SEM) images showed persistent CNCs sticking at the droplet’s contact line (Figure S6, Supporting Information). Such surface irregularities can pin the contact line of a drying droplet.^[21] A second array of sessile droplets was then applied to the same substrate and dried slowly under hexadecane. Once fully dried, the substrate was taken out from the hexadecane bath, rinsed in ethanol and blown dry with nitrogen gas. Rinsing with ethanol temporarily red-shifted the microfilms, with no sign of damage, but upon drying with nitrogen the microfilms blue-shifted back to their original color. In contrast, when freshly-prepared microfilms were immersed in water, the CNCs were redispersed, resulting in the loss of the microfilms.

Profilometry: The cross-sectional height profile of the microfilm, h , was measured by scanning across the sample using a stylus profilometer (DektakXT, Bruker) with a 12.5 μm tip radius at 4 mg force, with a resolution of 0.33 μm and a speed of 100 $\mu\text{m s}^{-1}$. To measure the profile of the optical path length, l_{opt} , reflectance spectra of CNC microfilms were acquired by microspectroscopy in RCP to isolate the thin-film interference fringes from the reflectance of the CNC nanoarchitecture. Thin-film interference imposes a sinusoidal variation on the reflectance according to^[32]

$$R(\lambda) = A \sin\left(\frac{4\pi}{\lambda} l_{\text{opt}} + B\right) + C \quad (1)$$

where $R(\lambda)$ is the measured reflectance at wavelength λ , and A , B , and C are free parameters varied to give the best fit without affecting the oscillation frequency. The cross-sectional and optical path length profiles were in excellent agreement, with a scaling factor corresponding to the average refractive index, $\bar{n} = \frac{l_{\text{opt}}}{h} = 1.55$.

Temperature and Humidity Control: As shown in Figure S11 (Supporting Information), the sample was placed in a heating chamber (THMS600, Linkam Scientific) with the humidity of the inlet

gas measured by an electronic humidity sensor (TSP01, Thorlab, $\pm 1\%$ between 20% and 80% RH, otherwise $\pm 3\%$ error). For the temperature-controlled study, dry nitrogen gas was flushed into the chamber while the sample temperature was cycled three times from 20 to 60 °C. For the absolute humidity experiment, the sample was heated from 20 to 60 °C, while the supplied water vapor was kept constant at 12.94 g m⁻³. For the relative humidity-controlled study, dry and wet nitrogen gas flows were mixed such that the relative humidity could be tuned between 0% and 75% at 20 °C. To investigate the response to large changes in relative humidity, the tester exhaled onto the sample until a significant color change was observed. To recover the color, the sample was blown with dry nitrogen gas.

Supporting Information

Supporting Information is available from the Wiley Online Library or from the author. Additional data relating to this publication is available from the University of Cambridge data repository (<https://doi.org/10.17863/CAM.25747>).

Acknowledgements

This work was supported by the European Research Council [ERC-2014-STG H2020 639088], the BBSRC David Phillips Fellowship [BB/K014617/1], the EPSRC [EP/L016087/1, EP/R511675/1, EP/L015978/1, EP/N016920/1], and the Winton Programme for the Physics of Sustainability. The authors thank Dr. Hsin-Ling Liang and Dr. Ziyi Yu for fabrication of the photolithography master and Prof. Chris Abell for the generous use of his laboratory.

Conflict of Interest

The authors declare no conflict of interest.

Keywords

cellulose nanocrystals, cholesteric liquid crystals, colloidal self-assembly, humidity sensors, sessile droplets

Received: July 2, 2018

Revised: July 23, 2018

Published online:

- [1] H. Sehaqui, Q. Zhou, O. Ikkala, L. A. Berglund, *Biomacromolecules* **2011**, *12*, 3638.
- [2] M. S. Toivonen, O. D. Onelli, G. Jacucci, V. Lovikka, O. J. Rojas, O. Ikkala, S. Vignolini, *Adv. Mater.* **2018**, *30*, 1704050.
- [3] R. Bardet, F. Rousset, S. Coindeau, N. Belgacem, J. Bras, *Carbohydr. Polym.* **2015**, *122*, 367.
- [4] M. K. Khan, A. Bsoul, K. Walus, W. Y. Hamad, M. J. Maclachlan, *Angew. Chem., Int. Ed.* **2015**, *54*, 4304.
- [5] X. M. Dong, T. Kimura, J.-F. Revol, D. G. Gray, *Langmuir* **1996**, *12*, 2076.
- [6] C. Schütz, M. Agthe, A. B. Fall, K. Gordeyeva, V. Guccini, M. Salajková, T. S. Plivelic, J. P. F. Lagerwall, G. Salazar-Alvarez, L. Bergström, *Langmuir* **2015**, *31*, 6507.
- [7] R. M. Parker, G. Guidetti, C. A. Williams, T. Zhao, A. Narkevicius, S. Vignolini, B. Frka-Petesic, *Adv. Mater.* **2018**, *30*, 1704477.
- [8] B. Frka-Petesic, G. Guidetti, G. Kamita, S. Vignolini, *Adv. Mater.* **2017**, *29*, 1701469.
- [9] A. G. Dumanli, G. Kamita, J. Landman, H. van der Kooij, B. J. Glover, J. J. Baumberg, U. Steiner, S. Vignolini, *Adv. Opt. Mater.* **2014**, *2*, 646.
- [10] M. Ličen, B. Majaron, J. Noh, C. Schütz, L. Bergström, J. Lagerwall, I. Drevenšek-Olenik, *Cellulose* **2016**, *23*, 3601.
- [11] B. D. Wilts, A. G. Dumanli, R. Middleton, P. Vukusic, S. Vignolini, *APL Photonics* **2017**, *2*, 040801.
- [12] R. M. Parker, B. Frka-Petesic, G. Guidetti, G. Kamita, G. Consani, C. Abell, S. Vignolini, *ACS Nano* **2016**, *10*, 8443.
- [13] Y. Li, J. J. Suen, E. Prince, E. M. Larin, A. Klinkova, H. Thérien-Aubin, S. Zhu, B. Yang, O. D. Lavrentovich, E. Kumacheva, *Nat. Commun.* **2016**, *7*, 12520.
- [14] A. A. Darhuber, S. M. Troian, S. Wagner, *J. Appl. Phys.* **2001**, *90*, 3602.
- [15] W. Feng, L. Li, X. Du, A. Welle, P. A. Levkin, *Adv. Mater.* **2016**, *28*, 3202.
- [16] S. P. R. Kobaku, A. K. Kota, D. H. Lee, J. M. Mabry, A. Tuteja, *Angew. Chem., Int. Ed.* **2012**, *51*, 10109.
- [17] S. Beck, J. Bouchard, R. Berry, *Biomacromolecules* **2011**, *12*, 167.
- [18] T. Wu, J. Li, J. Li, S. Ye, J. Wei, J. Guo, *J. Mater. Chem. C* **2016**, *4*, 9687.
- [19] G. Guidetti, S. Atifi, S. Vignolini, W. Y. Hamad, *Adv. Mater.* **2016**, *28*, 10042.
- [20] K. Yao, Q. Meng, V. Bulone, Q. Zhou, *Adv. Mater.* **2017**, *29*, 1701323.
- [21] R. D. Deegan, O. Bakajin, T. F. Dupont, G. Huber, S. R. Nagel, T. A. Witten, *Nature* **1997**, *389*, 827.
- [22] R. D. Deegan, *Phys. Rev. E* **2000**, *61*, 475.
- [23] X. Mu, D. G. Gray, *Langmuir* **2014**, *30*, 9256.
- [24] D. G. Gray, X. Mu, *Materials* **2015**, *8*, 7873.
- [25] X. Mu, D. G. Gray, *Cellulose* **2015**, *22*, 1103.
- [26] P. Wang, W. Y. Hamad, M. J. Maclachlan, *Nat. Commun.* **2016**, *7*, 11515.
- [27] Y. Li, E. Prince, S. Cho, A. Salari, Y. Mosaddeghian Golestani, O. D. Lavrentovich, E. Kumacheva, *Proc. Natl. Acad. Sci. USA* **2017**, *114*, 2137.
- [28] A. G. Dumanli, H. M. Van Der Kooij, G. Kamita, E. Reisner, J. J. Baumberg, U. Steiner, S. Vignolini, *ACS Appl. Mater. Interfaces* **2014**, *6*, 12302.
- [29] N. Bumbudsanpharoke, W. Lee, U. Chung, S. Ko, *Cellulose* **2018**, *25*, 305.
- [30] T. Lu, H. Pan, J. Ma, Y. Li, S. W. Bokhari, X. Jiang, S. Zhu, D. Zhang, *ACS Appl. Mater. Interfaces* **2017**, *9*, 18231.
- [31] M. Giese, L. K. Blusch, M. K. Khan, W. Y. Hamad, M. J. Maclachlan, *Angew. Chem., Int. Ed.* **2014**, *53*, 8880.
- [32] M. Quinten, *A Practical Guide to Optical Metrology for Thin Films*, Wiley-VCH Verlag & Co. KGaA, Weinheim **2012**.